LANGMUIR

pubs.acs.org/Langmuir Article

Using Simulation to Understand the Role of Titration on the Stability of a Peptide–Lipid Bilayer Complex

Violetta Burns and Blake Mertz*

Cite This: https://dx.doi.org/10.1021/acs.langmuir.0c02038 Read Online

ACCESS | Metrics & More | Article Recommendations | Supporting Information

ABSTRACT: The pH-low insertion peptide (pHLIP) is an anionic membrane-active peptide with promising potential for applications in imaging of cancer tumors and targeted delivery of chemotherapeutics. The key advantage of pHLIP lies in its acid sensitivity: in acidic cellular environments, pHLIP can insert unidirectionally into the plasma membrane. Partitioning–folding coupling is triggered by titration of the acidic residues in pHLIP, transforming pHLIP from a hydrophilic to a hydrophobic peptide. Despite this knowledge, the reverse pathway that leads to exit of the peptide from the plasma membrane is poorly understood. Our hypothesis is that sequential deprotonation of pHLIP is a prerequisite for exit of the peptide from the plasma membrane. We carried out molecular dynamics (MD) simulations to characterize the effect that deprotonation of the acidic residues of pHLIP has on the stability of the peptide when inserted into a model lipid bilayer of 1-palmitoyl-2-oleoyl-*sn*-3-phosphocholine (POPC). Initiation of the exit mechanism is facilitated by a complex relationship between the peptide, bulk solvent, and the membrane environment. As the N-terminal acidic residues of pHLIP are deprotonated, localized loss of helicity drives unfolding of the peptide and more pronounced interactions with the bilayer at the lipid–water interface. Deprotonation of the C-terminal acidic residues (D25, D31, D33, and E34) leads to further loss of secondary structure distal from the C-terminus, as well as formation of a water channel that stabilizes the orientation of pHLIP parallel to the membrane normal. Together, these results help explain how stabilization of intermediates between the surface-bound and inserted states of pHLIP occur and provide insights into rational design of pHLIP variants with modified abilities of insertion.

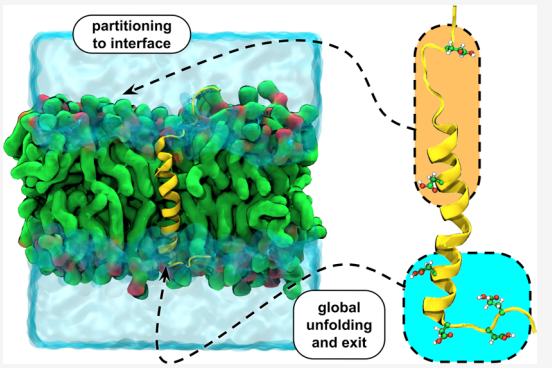

INTRODUCTION

The pH-Low Insertion Peptide (pHLIP) is a membrane-active peptide that in recent years has shown much promise in clinical applications to treat cancer.[1,2] pHLIP was originally derived from helix C of bacteriorhodopsin and was discovered during a mechanistic study on the folding of membrane proteins.[3] The peptide exists in a coiled conformation in solution (state I). Upon encountering a membrane surface, it spontaneously binds (state II). Folding and insertion is triggered by protonation of the acidic residues in pHLIP (E3, D14, D25, D31, D33, and E34), with insertion occurring unidirectionally (state III) (Figure 1). Initial studies posited that protonation of D14 and D25, the acidic residues in the transmembrane segment of pHLIP, were the driving factors in the acid sensitivity of the peptide.[3−5] Subsequent studies have shown that folding and insertion of pHLIP is much more nuanced, with protonation occurring in a nonsequential and nonbinary manner.[6,7]

In particular, it has been difficult to harmonize experimental and computational studies to produce a consensus on particular aspects of the binding, folding, and insertion mechanism of pHLIP. Fluorescence and circular dichroism (CD) spectroscopic studies have been used extensively to establish that binding of pHLIP is most effective in PC-only lipid systems, and that anionic lipid headgroups can lead to shallower binding of pHLIP.[4,8−11] Site-specific fluorescence labeling revealed that particular segments of pHLIP exhibit a characteristic pK_a of insertion,[7] lending support to a multistep model of insertion that was initially suggested by stopped-flow kinetics studies on the insertion and exit mechanisms of pHLIP.[5] To date, solid-state NMR has provided an exquisite level of detail on the insertion mechanism of pHLIP; the peptide can coexist in a surface-bound and transmembrane inserted state at slightly acidic pH,[12] indicating that several conformational intermediates exist in the insertion pathway. The next study from Qiang, An, and co-workers established that protonation of aspartic acids in the state II → state III transition was not sequential and did not depend solely on D14 and D25; rather, D31 and D33 were protonated first, followed by D25 and D14.[6] Fluorescence quenching experi-

Received: July 15, 2020
Revised: September 22, 2020
Published: September 29, 2020

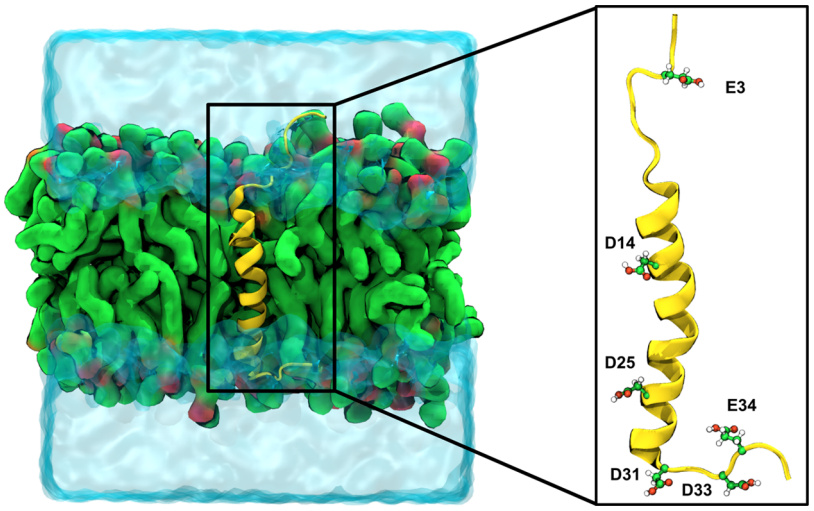

Figure 1. Overview of the systems studied. Left: Snapshot of pHLIP (yellow) folded and inserted into a 1-palmitoyl-2-oleoyl-*sn*-3-phosphocholine (POPC) bilayer (surface, green, and red). Inset: Close-up of pHLIP highlighting the acidic residues that are either protonated or deprotonated in this study.

ments also showed that the membrane environment underwent a significant degree of perturbation at intermediate pH values, with penetration of water molecules into the hydrophobic interior.[6] Most recently, Qiang, An, and co-workers were able to correlate thermodynamic intermediate states with protonation of specific residues in pHLIP, confirming that protonation of D31 and D33 are the trigger for partitioning into the bilayer as the initial step in insertion as well as driving conformational changes in the N-terminal half of the peptide.[13] Equilibrium molecular dynamics (MD) simulations have been effective in providing detailed descriptions of pHLIP in solution[14] and binding of pHLIP,[15,16] showing that pHLIP can undergo partial folding in the solution and the surface-bound state without protonation of key acidic residues. To date, the most notable characterization of the inserted state of pHLIP has been a constant pH MD study on pHLIP and the L16H variant.[17] There it was shown that deprotonation of D14 was the determining factor in destabilization of positioning of pHLIP within the bilayer, shifting the peptide to a more surface-bound position.

Although the mechanism of folding and insertion of pHLIP is now more fully characterized, the molecular interactions that govern the reverse pathway (unfolding and exit) are poorly understood. The acquisition of this detailed knowledge has implications in relating the behavior of pHLIP to biomedically relevant phenomena, such as residence time of pHLIP in tumor tissue. Determination of the effect of deprotonation of specific acidic residues in pHLIP on the stability of the inserted state is significant to this understanding: we know that the insertion and exit pathways are thermodynamically equivalent,[13] but kinetics studies indicate that these pathways are independent from one another.[5] We hypothesize that deprotonation of the N-terminal acidic residues are a prerequisite for unfolding of pHLIP, while deprotonation of C-terminal residues are key to anchoring pHLIP in state III. Furthermore, we wanted to probe the role of internal hydration of the bilayer in state III, despite evidence that pHLIP does not create a pore in the inserted state.[4] To test these hypotheses, we carried out equilibrium molecular dynamics (MD) simulations of pHLIP in state III, sequentially deprotonating the acidic residues from the N- to the C-terminus. Despite the fact that sequential deprotonation of pHLIP may not reflect the exact order of deprotonation in the state III → state II transition, it nonetheless provides a comparative basis between the different acidic residues in pHLIP. Interestingly, we found that although deprotonation of N-terminal acidic residues are important to initial unfolding of the peptide, the protonation state of the C-terminal acidic residues hold the key to stabilization of the proteolipid complex.

COMPUTATIONAL METHODS

System Setup. Coordinates for pHLIP (amino acid sequence GGEQNPIYWARYADWLFTTPLLLLDLALLVDADEGT) were obtained from bacteriorhodopsin (PDB 1FBB) by selecting residues 72−107 and mutating residue 105 from Gln to Glu. pHLIP was inserted as a transmembrane helix into a 1-palmitoyl-2-oleoyl-*sn*-3-phosphocholine (POPC) bilayer at a 150:1 lipid:peptide ratio, with 50 waters per lipid and 100 mM NaCl, using the replacement method in the charmm-gui web server.[18] Each system was designed with sequential deprotonation of the acidic residues in pHLIP from the N-terminus to the C-terminus of the peptide (Table 1). Although this progression of protonation states and system setup is not completely consistent with what we do know about the insertion of pHLIP,[6,7,13,17] it allows for a simplified comparison between the individual acidic residues in pHLIP (without the benefit of an enhanced sampling technique such as constant pH MD) as well as extension to time scales that facilitate equilibration of the bilayer surrounding the peptide.[19,20]

Table 1. List of Protonation States of pHLIP in This Study

label	deprotonated residues	net charge of pHLIP
none	none	+1
N_t-E3	E3	0
N_t-D14	E3, D14	−1
N_t-D25	E3, D14, D25	−2
N_t-D31	E3, D14, D25, D31	−3
N_t-D33	E3, D14, D25, D31, D33	−4
N_t-C_t	E3, D14, D25, D31, D33, E34	−5

MD Simulations. All systems generated from charmm-gui were equilibrated for 50 ns with a 2 fs timestep in the *NPT* ensemble (P = 1 atm, T = 310 K) using the Langevin thermostat and Nosé−Hoover

https://dx.doi.org/10.1021/acs.langmuir.0c02038
Langmuir XXXX, XXX, XXX−XXX

barostat in NAMD 2.13.[21] The charmm36 force fields for lipids and proteins, and the TIP3P model for water,[22−24] were used. Standard cutoffs for nonbonded forces consistent with charmm force fields (10 Å switching distance and 12 Å cutoff) were used. After equilibration, coordinates from the last frame of the trajectory were converted to the AMBER force field topology (ff14SB, OPC, and lipid17[25−27]) to be used in production runs. Minimization and equilibration of the Amber-based system was carried out for 1 ns with a 2 fs timestep in the *NPT* ensemble (T = 310 K, P = 1 atm) using the Langevin thermostat and Monte Carlo barostat with semianisotropic pressure coupling to maintain the aspect ratio of the *xy*-plane of the lipid bilayer, all in the sander MD engine in AMBER18.[28] An 8 Å cutoff for nonbonded forces was used, consistent with Amber force fields. Production runs had the same settings as minimization and equilibration, utilizing the GPU version of pmemd in AMBER18.[28,29] Stabilization of general positioning of pHLIP in the bilayer was monitored by measuring the z-position of D14 and D25 for each of the respective protonation states (Figure S1). Simulations were run in triplicate for an aggregate time of 15 μs per protonation state.

Analysis. Analysis was performed using VMD,[30] cpptraj in AmberTools,[28] LOOS,[31] and in-house scripts. VMD and gnuplot[32] were used to render all snapshots and plot data.

RESULTS AND DISCUSSION

Deprotonation of Acidic Residues Can Lead to Either Localized or Distal Loss in Helicity. To analyze our hypothesis that deprotonation of pHLIP in state III leads to destabilization of the proteolipid complex, we examined the relationship of deprotonation to helicity of pHLIP. As we increased the degree of deprotonation of acidic residues, we observed a localized loss of helicity (Figure 2A). However, deprotonation of the C-terminal acidic residues (in particular, D25, D31, and E34) has a more distal effect, decreasing helicity from residues 9−15. This behavior could be related to the fact that deprotonation of the C-terminal acidic residues (D31, D33, E34, and the carboxy terminus) is the most likely protonation state of the inserted TM conformation of pHLIP.[13,17] In general, helicity decreases with an increase in deprotonation, specifically in residues 9−13 in the N-terminus and residues 17−29 in the C-terminus. This loss of helicity indicates a decrease in the stability of the peptide in the membrane as a function of the degree of deprotonation. Although we do not observe a direct effect between the deprotonated residue and localized changes in helicity, the overall helicity of pHLIP clearly shows a direct correlation between protonation and helicity. Helicity decreases from nearly half of the peptide in a folded helical state when all acidic residues are protonated to less than 30% helicity when all acidic residues are deprotonated (Figures 2B and S2).

Unfolding of the helical segment of pHLIP leads to global changes in the peptide as well. Radius of gyration (r_g) can be used as a general indicator of this helix-to-coil transition. As pHLIP is deprotonated, r_g increases, indicating that the entire peptide is unfolding while still embedded in the bilayer (Figure 3). Interestingly, upon deprotonation of all acidic residues, r_g decreases, consistent with partial recapture of helicity in the C-terminal half of the transmembrane segment. This indicates the potential for cooperativity between deprotonation of D31, D33, and E34 and refolding of the C-terminal segment of residues that is exposed to bulk solvent in the cytoplasm.

pHLIP Repositions in the Bilayer in Distinct Ways to Compensate for Deprotonation. Upon identifying that deprotonation of acidic residues triggers unfolding in pHLIP, we turned our attention to the role that the bilayer plays in this

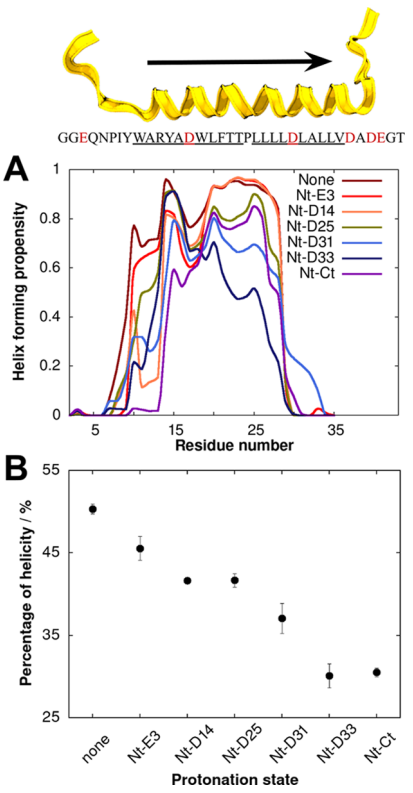

Figure 2. Sequential deprotonation of pHLIP leads to localized and global changes in helicity. Top: Representative conformation of pHLIP in the fully folded state. Primary amino acid sequence of pHLIP, with putative transmembrane segment underlined. (A) Per-residue helicity of pHLIP as a function of protonation state. (B) Total helical content of pHLIP as a function of protonation state.

mechanism. A complex relationship exists between the two components that maintain bilayer stability while also facilitating the unfolding of pHLIP. The helical tilt angle gradually decreases with sequential deprotonation of pHLIP, proceeding from a maximum of 32−21° in the fully deprotonated state (Figure 4A). This shift is actually manifested in contrasting motions within pHLIP: upon deprotonation of the first C-terminal acidic residue (D25), a sharp increase occurs in the tilt angle of the N-terminal half of pHLIP, initiating movement of this segment of the peptide to a position more parallel to the lateral plane of the lipid bilayer (Figure 4B). However, the tilt angle of the C-terminal half of pHLIP notably decreases, also upon deprotonation of D25 (Figure 4C). The compensatory motions of the two TM segments are captured by the hinge angle centered around the kink at P20, where we observe a slight increase in the angle—as the N-terminal segment becomes more parallel to the bilayer surface and the C-terminal segment becomes more parallel to the bilayer normal, pHLIP becomes slightly more linear (Figure 4D).

Closer examination of the interactions between pHLIP and the bilayer reveals that individual residues and groups of residues play a specific role in destabilization of the proteolipid complex. First, a clear demarcation exists in the positioning of the TM helix upon deprotonation of any C-terminal acidic residues (Figure 5). Second, deprotonation of C-terminal acidic residues (D25, D31, D33, and E34) leads to protrusion of the C-terminus from the bilayer. This effectively switches these residues from nonpolar to hydrophilic side chains,

https://dx.doi.org/10.1021/acs.langmuir.0c02038
Langmuir XXXX, XXX, XXX−XXX

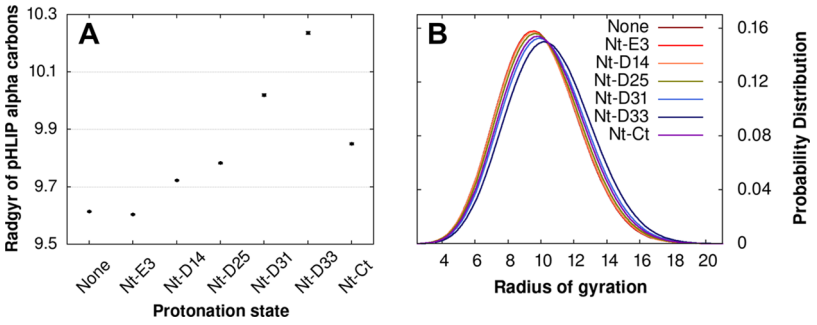

Figure 3. Deprotonation of acidic residues triggers the expansion of pHLIP. (A) Average radius of gyration (r_g) of the TM segment of pHLIP as a function of deprotonation of acidic residues. (B) Distribution of r_g of the TM segment of pHLIP as a function of deprotonation of acidic residues.

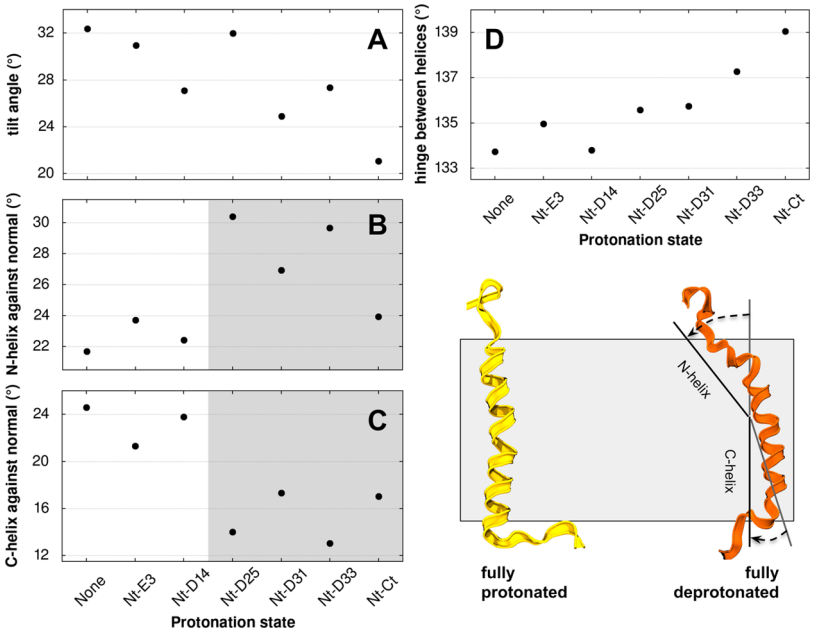

Figure 4. Hydrophobic effect leads to compensating motions of N- and C-terminal halves of pHLIP TM helix as acidic residues are progressively deprotonated. (A) Helix tilt angle with respect to the membrane normal, as defined by the vector from residues 8−30 in pHLIP. (B) Helix tilt angle with respect to the membrane normal, as defined by the vector from residues 8−19 in pHLIP. (C) Helix tilt angle with respect to the membrane normal, as defined by the vector from residues 21−30 in pHLIP. (D) Hinge angle as measured between the vectors formed by the N-terminal (residues 10−19) and C-terminal (residues 21−30) halves of the transmembrane (TM) helix of pHLIP. Lower right: schematic showing the corresponding change in the tilt angle of each TM segment of pHLIP as it is fully deprotonated.

stabilizing their position with respect to the interior of the bilayer. Third, an increase in deprotonation also leads to partitioning of the N-terminal segment of pHLIP (residues 1−8) into the headgroup region of the upper leaflet. This behavior could potentially stabilize the N-terminal position of pHLIP, compensating for the increased movement of the C-terminal half of the peptide as D25, D31, D33, and E34 are deprotonated.

Localized Destabilization of the Bilayer is Closely Coupled to Deprotonation of pHLIP and Hydration of the Hydrophobic Interior. The cooperative motions of pHLIP that occur as a function of deprotonation take place in concert with destabilization of the lipid bilayer. The radial distribution function (RDF) of water with respect to pHLIP reveals a stark contrast upon deprotonation of the C-terminal acidic residues: beginning with D25, a sharp increase in the RDF occurs, indicating an influx of waters into the hydrophobic interior of the bilayer (Figures 6A and S3A). If we count the frequency with which a water molecule enters the interior of the membrane, a similar trend emerges: upon deprotonation of D25, a sharp spike (almost 3 orders of magnitude) is observed in the diffusion of water into the bilayer interior (Figure 6B). The residency time of waters in the bilayer also reflects the shift in the diffusive behavior of waters as the bilayer becomes destabilized, showing that when the C-terminal residues of pHLIP are deprotonated, the majority of waters spend a short time (<20 ns) in the hydrophobic region of the bilayer, indicating fast exchange of water molecules with bulk solvent. In contrast, when fewer residues are deprotonated, waters can spend >40 ns in the bilayer, indicating a snorkeling effect that is stabilized by interactions with pHLIP (Figure 6C). Finally, deprotonation of pHLIP also leads to global disruption of the bilayer, where we observe that the entire lipid patch has a noticeably lower molecular order parameter (MOP) upon deprotonation of D25, well beyond the second and third shell of lipids (Figure 6D). Visualization of the water density in our simulations paints a similar picture. As the N-terminal acidic residues are deprotonated, there is a slight increase in the influx of water molecules from bulk extracellular solvent, but it is not until

https://dx.doi.org/10.1021/acs.langmuir.0c02038
Langmuir XXXX, XXX, XXX−XXX

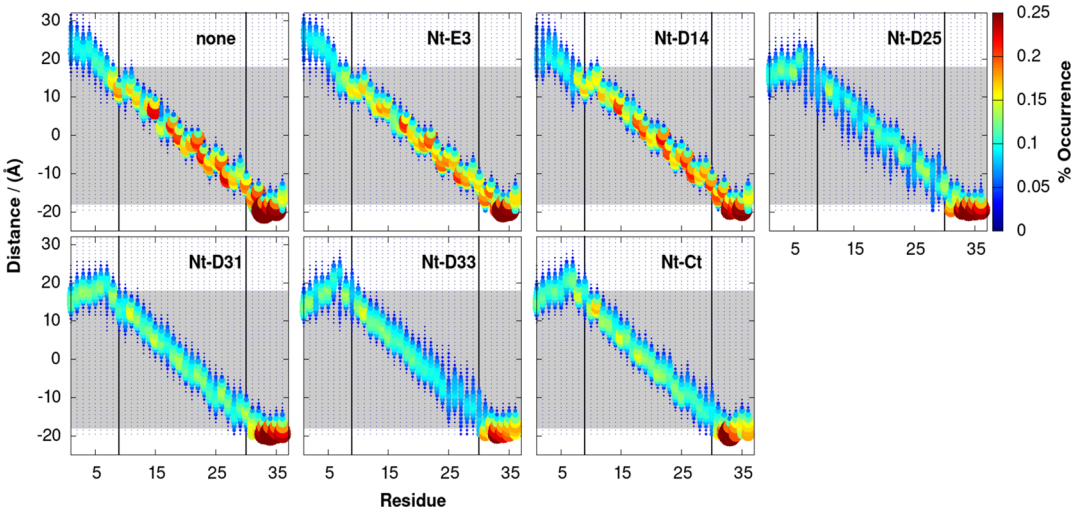

Figure 5. Deprotonation has subtle localized and global effects on positioning of pHLIP in state III. Per-residue distance distribution of pHLIP with respect to the midplane of the POPC bilayer (zero corresponds to the projection onto the *z*-axis of the center of mass of the bilayer). The heat bar indicates the probability of per-residue distance. The thick black vertical lines indicate the boundaries of the TM segment of pHLIP.

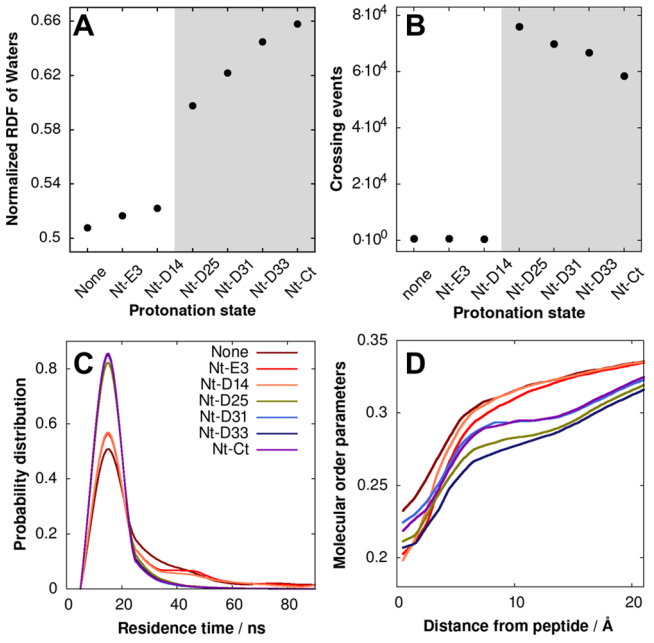

Figure 6. Destabilization of the hydrophobic interior of the bilayer is coupled to deprotonation of pHLIP in state III. (A) Maximum value of the first shell of the radial distribution function (RDF) of water with respect to pHLIP. (B) Explicit count of the number of times a water molecule diffuses into the membrane interior, shown as the number of crossing events. (C) Probability distribution of the time a given water molecule spends in the hydrophobic region of the bilayer. (D) Molecular order parameter (MOP) of pHLIP.

D25 is deprotonated that the peptide−bilayer interface is disrupted to the point that water molecules can snorkel into the bilayer interior, forming a continuous pore connecting bulk solvent from the exterior and interior of the cell (Figure 7).

All other measurements of the bilayer paint a similar picture: deprotonation of D25 and subsequent C-terminal acidic residues are the key to facilitating migration of pHLIP toward the outer leaflet of the membrane. There is a clear transition from more ordered to less ordered acyl chains upon deprotonation of D25 (Figure S3B,C). This disorder in the interior of the bilayer manifests itself in a noticeable increase in area per lipid (Figure S3D) and corresponding decrease in bilayer thickness (Figure S3E). Although pHLIP remains in a TM state in all of our simulations, the decrease in bilayer thickness corresponding to deprotonation of D25 is more pronounced in the upper leaflet than the lower leaflet (Figure S3F,G). In addition to equilibrium biophysical properties of the bilayer, we observe that insertion of pHLIP significantly alters the lateral diffusion of lipids and their motions along the bilayer normal in the fully inserted state. The lateral diffusion of lipids is noticeably slower when pHLIP is fully protonated (Figure S4A), as well as reducing the mean-squared displacement (MSD) of PC headgroups in half (Figure S4B). Overall, this indicates that pHLIP in the fully inserted state has both a localized and distal effect of ordering the membrane.

Implications of Results on Understanding of pHLIP in State III. Although the use of equilibrium MD simulations does not allow us to model the reversible protonation and deprotonation events that drive the transition of pHLIP from the folded, inserted state to the unfolded, surface-bound state, it does provide valuable insights into how deprotonation of acidic residues leads to destabilization of pHLIP in state III. We observed both localized and distal effects on the helicity of pHLIP when deprotonating acidic residues. It is clear that unfolding of the N-terminal half of pHLIP is a prerequisite for exit, but multiple factors can tune this process. This particular result is not unexpected, as a recent constant pH MD study on pHLIP in state III revealed that the N-terminal half of pHLIP migrates to the bilayer−water interface at neutral pH.[17] Calculation of the pK_a of acidic residues revealed that D14 was the trigger for this migration, and although they were unable to resolve the pK_a of D25, it is expected that deprotonation of D25 also contributed to this surface-bound state, in agreement with our results. What is noticeably different in our simulations is the restoration of helicity in the C-terminal half of pHLIP upon deprotonation of all acidic residues, including E34. A possible explanation for this localized increase in folding lies in the N-terminal segment of pHLIP: we observed a decrease in the overall and C-terminal tilt angles of pHLIP (i.e., less surface-bound and more inserted). This shift in the orientation of the peptide helps

https://dx.doi.org/10.1021/acs.langmuir.0c02038
Langmuir XXXX, XXX, XXX−XXX

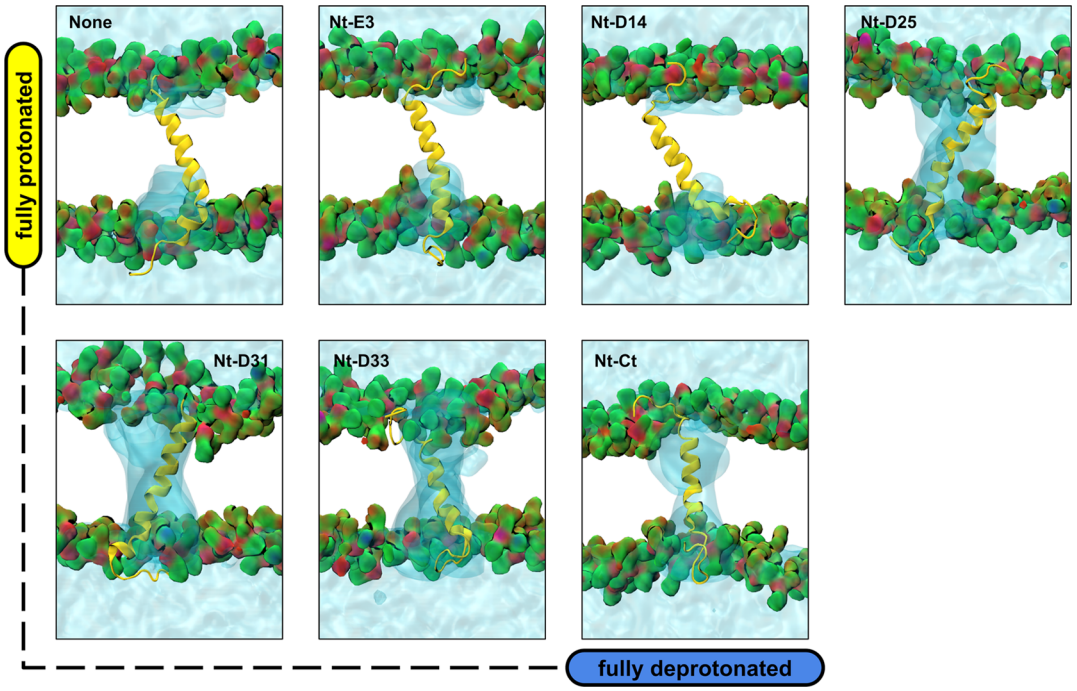

Figure 7. Deprotonation of acidic residues leads to penetration of water molecules into the interior of the bilayer. The volumetric representation of average water density for each protonation state in pHLIP. The average structure of pHLIP is used to show the gradual invasion of waters as pHLIP is sequentially deprotonated. Red and green surface: headgroups of upper and lower leaflets of POPC bilayer; blue surface: water; and yellow cartoon: pHLIP.

offset the migration of deprotonated E34 toward bulk solvent on the cytoplasmic side of the bilayer. The presence of R11 sandwiched between aromatic residues (Y8, W9, Y12, and W15) helps facilitate this shift: previous studies on model peptides and pHLIP showed that the location of an arginine residue slightly off-center in the transmembrane segment, in close proximity to aromatic residues, allows the arginine side chain to snorkel toward the bilayer surface and interact with bulk solvent.[33] The transmembrane orientation can also interchange with a surface-bound orientation that is presumably stabilized by partitioning of aromatic side chains into the headgroup region of the membrane,[15,33] which is consistent with the transition between states II and III in pHLIP.

What appears to occur during deprotonation of pHLIP within the bilayer is a cooperative effect between R11 and the deprotonated acidic residues. These two groups act in concert to stabilize a localized deformation in the membrane. The guanidinium group of arginine is able to stabilize single-span peptides at the bilayer−water interface by forming a bidentate hydrogen bond with the phosphate moiety of the PC headgroup; this interaction is what leads to the snorkeling of the side chain toward the extracellular solvent.[34] In the context of membrane protein folding via the translocon, a shift of 1.2 Å of the arginine residue toward the bilayer−water interface lowers the free energy of membrane integration by 0.4 kcal/mol.[35]

Likewise, deprotonation of acidic residues helps trigger the state III → state II transition of pHLIP. One way in which this is accomplished is by extending the penetration of waters into the interior of the bilayer. Temperature-accelerated MD (TAMD) simulations have been able to demonstrate that negatively charged acidic residues recruit waters into the membrane to decrease the energy penalty for translocation of transmembrane loops across the membrane.[36] Our results are consistent with this study, showing a sharp increase in hydration of the bilayer interior upon sequential deprotonation of D25, D31, D33, and E34. Beginning with D25, there is a transition in the behavior of water molecules interacting with the bilayer—the majority of water molecules freely diffuse between bulk solvent and the bilayer, leading to a localized deformation of the proteolipid complex. This observation is also supported by time-resolved Fourier transform infrared (FTIR) spectroscopic and MD studies on pHLIP in state III, where it was determined that the C-terminal residues of pHLIP were more solvent-exposed in state III.[37,38] The hypothesis that the C-terminus of pHLIP extends out of the inner plasma membrane and into the cytoplasmic solvent,[6,17] which would require the C-terminal acidic residues (D31, D33, and E34) to be deprotonated, is also in agreement with this observation. In addition to water penetration, divalent cations can play a role in stabilizing these intermediates; physiological concentrations of calcium were shown to increase the pK_a of insertion well above neutral pH.[39] It was hypothesized that Ca^{2+} ions act to coordinate between deprotonated acidic residues in pHLIP and lipid headgroups, stabilizing intermediates between states II and III and lowering the energy barrier for folding and insertion. In essence, the positioning of the N-terminal half of pHLIP to a more surface-bound orientation stabilizes the rest of the peptide during the exit process.[40]

The physicochemical properties of the membrane can have a noticeable effect on binding and insertion of pHLIP,[10,11,41,42] making it critical to obtain a detailed understanding of the relationship between pHLIP and the membrane environment. A key characteristic of pHLIP is that it acts as a monomer without forming a pore.[4] However, it is clear from solid-state NMR and fluorescence experiments that pHLIP perturbs the bilayer environment during insertion to the point that there is a significant influx of water into the bilayer,[6] and presumably

https://dx.doi.org/10.1021/acs.langmuir.0c02038
Langmuir XXXX, XXX, XXX−XXX

would do the same during exit. Our simulations provide ample evidence that this is indeed the case: a clear transition in the proteolipid complex occurs upon deprotonation of D25 and subsequent C-terminal acidic residues. This transition is localized with respect to invasion of water molecules into the bilayer interior, but is also propagated to the bulk region of the bilayer. Ordering of the bilayer chains is restored approximately 12−15 Å from pHLIP for all combinations of the N-terminal deprotonations, but this recovery does not occur with deprotonation of the C-terminal residues. The majority of perturbation to the bilayer appears to occur in the extracellular leaflet, where the N-terminal half of pHLIP undergoes considerable movement and transitions from a helical to a coiled conformation. This leads to a subsequent increase in area per lipid and a decrease in membrane thickness. More interesting is the effect of pHLIP on the diffusion of the bilayer; when pHLIP is fully inserted and protonated, lateral diffusion of the POPC lipids is decreased by a factor of 2 and fluctuations of the headgroups along the membrane normal are nearly half of their value compared to when pHLIP is fully deprotonated. This ordering of the lipid bilayer via the insertion of pHLIP does not exist for heterogeneous bilayers containing cholesterol (unpublished results), indicating that pHLIP has a similar effect to cholesterol or sphingomyelin in inducing localized ordering of the membrane.[19,43]

Conventional fluorescence and CD spectroscopy techniques led to the initial suggestion that pHLIP can reversibly interconvert between states I, II, and III upon a transition from a neutral pH to an acidic, membrane-bound environment.[3,4] Subsequent studies have shown that this mechanism is much more nuanced. Kinetics studies indicated that multiple substates exist, with distinct pathways for insertion and exit.[5,8,44] Solid-state NMR and fluorescence spectroscopy revealed that each of the acidic residues in pHLIP possesses a unique pK_a, with titration occurring in a nonlinear fashion,[6,7] as well as revealing that pHLIP exists in multiple states at slightly acidic pH.[6,13] In addition to these mechanistic studies, it has become clear that the function of pHLIP can be influenced by both the membrane environment and peptide composition. Non-PC lipids can prevent partitioning of pHLIP to form a stable membrane-bound complex;[9−11] physiological salt concentrations can decrease the propensity for pHLIP to insert into a membrane;[16] even shifting the location of acidic residues in pHLIP or substituting acidic residues with more potent non-natural amino acids can enhance the effectiveness of insertion.[8,45] How do our results provide additional insights into this seemingly simple, yet complex mechanism?

It is clear that each half of the transmembrane segment of pHLIP stabilizes the inserted state of the peptide in its own unique manner. From our previous[14,15] and current studies, we know that R11 and the surrounding aromatic residues (Y8, W9, Y12, and W15) play a critical role in stabilizing the partitioned and inserted states of pHLIP. As discussed above, arginine can play a key role in stabilizing interactions of a peptide with the bilayer proximal to the headgroups of phospholipids, and the presence of the aromatic residues adds to this stabilizing effect. Similar to what was observed by Machuqueiro and co-workers,[17] deprotonation of the N-terminal acidic residues leads to interconversion between inserted and surface-bound states. With respect to the C-terminal half of the transmembrane segment, the long stretch of nonpolar residues from position 21−30 anchors pHLIP within the membrane. Interestingly, deprotonation of the C-terminal acidic residues has an opposing effect: it stabilizes the C-terminus of pHLIP by making it more favorable for D31, D33, and E34 to remain exposed to bulk solvent from the cytoplasm while also accelerating the rate of unfolding of the N-terminal half of pHLIP. This mechanism is strikingly similar to the exit pathway that was suggested by Reshetnyak and co-workers in their first kinetics study of pHLIP.[5]

CONCLUSIONS

Our results provide a detailed picture of the early stages of exit of pHLIP from a lipid bilayer. This aspect of the pHLIP mechanism has often been overlooked, but is a key element to the fundamental understanding of pHLIP and the development of biomedical applications such as diagnostic imaging of tumors, which depend on intimate knowledge of residence times within tissues. As stated above, the function of pHLIP can be influenced by numerous factors; comprehensive understanding of the effects of these factors will require creative approaches, both experimental and computational. This initial study into the exit mechanism of pHLIP will serve as a solid foundation for comparison to other membrane environments and use of enhanced sampling techniques, which are currently underway in our lab. Ultimately, we expect that this will inform researchers in development of pHLIP variants and conjugates with imaging agents or small molecule drugs.

ASSOCIATED CONTENT

Supporting Information

The Supporting Information is available free of charge at https://pubs.acs.org/doi/10.1021/acs.langmuir.0c02038.

Analysis of distribution of type of secondary structure of pHLIP as a function of protonation, bilayer effects as a function of protonation of pHLIP, and mean-squared displacement of lipids as a function of protonation of pHLIP (PDF)

AUTHOR INFORMATION

Corresponding Author

Blake Mertz − *C. Eugene Bennett Department of Chemistry and WVU Cancer Institute, West Virginia University, Morgantown, West Virginia 26506, United States;* orcid.org/0000-0002-7677-0496; Phone: +1 304 293 9166; Email: blake.mertz@mail.wvu.edu

Author

Violetta Burns − *C. Eugene Bennett Department of Chemistry, West Virginia University, Morgantown, West Virginia 26506, United States*

Complete contact information is available at: https://pubs.acs.org/10.1021/acs.langmuir.0c02038

Author Contributions

V.B. and B.M. designed the research. V.B. carried out all simulations, and V.B. and B.M. analyzed the data. V.B. and B.M. wrote the article.

Notes

The authors declare no competing financial interest.

ACKNOWLEDGMENTS

The authors thank Mertz lab members, Fran Barrera, Chris Neale, Mike Crowley, and Alan Grossfield for invaluable feedback on our simulations and results. This work was

supported by the National Institutes of Health grant GMI20676 (V.B. and B.M.). Computational time was provided through West Virginia University Research Computing.

REFERENCES

(1) Viola-Villegas, N. T.; Carlin, S. D.; Ackerstaff, E.; Sevak, K. K.; Divilov, V.; Serganova, I.; Kruchevsky, N.; Anderson, M.; Blasberg, R. G.; Andreev, O. A.; Engelman, D. M.; Koutcher, J. A.; Reshetnyak, Y. K.; Lewis, J. S. Understanding the Pharmacological Properties of a Metabolic PET Tracer in Prostate Cancer. *Proc. Natl. Acad. Sci. U.S.A.* **2014**, *111*, 7254−7259.

(2) Burns, K. E.; Robinson, M. K.; Thévenin, D. Inhibition of Cancer Cell Proliferation and Breast Tumor Targeting of pHLIP−Monomethyl Auristatin E Conjugates. *Mol. Pharmaceutics* **2015**, *12*, 1250−1258.

(3) Hunt, J. F.; Rath, P.; Rothschild, K. J.; Engelman, D. M. Spontaneous, pH-Dependent Membrane Insertion of a Transbilayer α-Helix. *Biochemistry* **1997**, *36*, 15177−15192.

(4) Reshetnyak, Y. K.; Segala, M.; Andreev, O. A.; Engelman, D. M. A Monomeric Membrane Peptide That Lives in Three Worlds: In Solution, Attached to, and Inserted across Lipid Bilayers. *Biophys. J.* **2007**, *93*, 2363−2372.

(5) Andreev, O. A.; Karabadzhak, A. G.; Weerakkody, D.; Andreev, G. O.; Engelman, D. M.; Reshetnyak, Y. K. pH (Low) Insertion Peptide (pHLIP) Inserts across a Lipid Bilayer as a Helix and Exits by a Different Path. *Proc. Natl. Acad. Sci. U.S.A.* **2010**, *107*, 4081−4086.

(6) Hanz, S. Z.; Shu, N. S.; Qian, J.; Christman, N.; Kranz, P.; An, M.; Grewer, C.; Qiang, W. Protonation-Driven Membrane Insertion of a pH-Low Insertion Peptide. *Angew. Chem., Int. Ed.* **2016**, *55*, 12376−12381.

(7) Scott, H. L.; Westerfield, J. M.; Barrera, F. N. Determination of the Membrane Translocation pK of the pH-Low Insertion Peptide. *Biophys. J.* **2017**, *113*, 869−879.

(8) Karabadzhak, A. G.; Weerakkody, D.; Wijesinghe, D.; Thakur, M. S.; Engelman, D. M.; Andreev, O. A.; Markin, V. S.; Reshetnyak, Y. K. Modulation of the pHLIP Transmembrane Helix Insertion Pathway. *Biophys. J.* **2012**, *102*, 1846−1855.

(9) Scott, H. L.; Nguyen, V. P.; Alves, D. S.; Davis, F. L.; Booth, K. R.; Bryner, J.; Barrera, F. N. The Negative Charge of the Membrane Has Opposite Effects on the Membrane Entry and Exit of pH-Low Insertion Peptide. *Biochemistry* **2015**, *54*, 1709−1712.

(10) Kyrychenko, A.; Vasquez-Montes, V.; Ulmschneider, M. B.; Ladokhin, A. S. Lipid Headgroups Modulate Membrane Insertion of pHLIP Peptide. *Biophys. J.* **2015**, *108*, 791−794.

(11) Vasquez-Montes, V.; Gerhart, J.; King, K. E.; Thévenin, D.; Ladokhin, A. S. Comparison of Lipid-Dependent Bilayer Insertion of pHLIP and Its P20G Variant. *Biochim. Biophys. Acta, Biomembr.* **2018**, *1860*, 534−543.

(12) Shu, N. S.; Chung, M. S.; Yao, L.; An, M.; Qiang, W. Residue-Specific Structures and Membrane Locations of pH-Low Insertion Peptide by Solid-State Nuclear Magnetic Resonance. *Nat. Commun.* **2015**, *6*, No. 7787.

(13) Otieno, S. A.; Hanz, S. Z.; Chakravorty, B.; Zhang, A.; Klees, L. M.; An, M.; Qiang, W. pH-Dependent Thermodynamic Intermediates of pHLIP Membrane Insertion Determined by Solid-State NMR Spectroscopy. *Proc. Natl. Acad. Sci. U.S.A.* **2018**, *115*, 12194−12199.

(14) Gupta, C.; Mertz, B. Protonation Enhances the Inherent Helix-Forming Propensity of pHLIP. *ACS Omega* **2017**, *2*, 8536−8542.

(15) Gupta, C.; Ren, Y.; Mertz, B. Cooperative Nonbonded Forces Control Membrane Binding of the pH-Low Insertion Peptide pHLIP. *Biophys. J.* **2018**, *115*, 2403−2412.

(16) Westerfield, J.; Gupta, C.; Scott, H. L.; Ye, Y.; Cameron, A.; Mertz, B.; Barrera, F. N. Ions Modulate Key Interactions between pHLIP and Lipid Membranes. *Biophys. J.* **2019**, *117*, 920−929.

(17) Vila-Viçosa, D.; Silva, T. F. D.; Slaybaugh, G.; Reshetnyak, Y. K.; Andreev, O. A.; Machuqueiro, M. Membrane-Induced pKa Shifts in Wt-pHLIP and Its L16H Variant. *J. Chem. Theory Comput.* **2018**, No. 3289.

(18) Jo, S.; Kim, T.; Iyer, V. G.; Im, W. CHARMM-GUI: A Web-Based Graphical User Interface for CHARMM. *J. Comput. Chem.* **2008**, *29*, 1859−1865.

(19) Sodt, A. J.; Sandar, M. L.; Gawrisch, K.; Pastor, R. W.; Lyman, E. The Molecular Structure of the Liquid-Ordered Phase of Lipid Bilayers. *J. Am. Chem. Soc.* **2014**, *136*, 725−732.

(20) Pino-Angeles, A.; Lazaridis, T. Effects of Peptide Charge, Orientation, and Concentration on Melittin Transmembrane Pores. *Biophys. J.* **2018**, *114*, 2865−2874.

(21) Melo, M. C. R.; Bernardi, R. C.; Rudack, T.; Scheurer, M.; Riplinger, C.; Phillips, J. C.; Maia, J. D. C.; Rocha, G. B.; Ribeiro, J. V.; Stone, J. E.; Neese, F.; Schulten, K.; Luthey-Schulten, Z. NAMD Goes Quantum: An Integrative Suite for Hybrid Simulations. *Nat. Methods* **2018**, *15*, 351−354.

(22) Klauda, J. B.; Venable, R.; Freites, J. A.; O'Connor, J. W.; Tobias, D. J.; Mondragon-Ramirez, C.; Vorobyov, I.; MacKerell, A. D.; Pastor, R. W. Update of the CHARMM All-Atom Additive Force Field for Lipids: Validation on Six Lipid Types. *J. Phys. Chem. B* **2010**, *114*, 7830−7843.

(23) Best, R. B.; Zhu, X.; Shim, J.; Lopes, P. E. M.; Mittal, J.; Feig, M.; MacKerell, A. D. Optimization of the Additive CHARMM All-Atom Protein Force Field Targeting Improved Sampling of the Backbone ϕ, ψ and Side-Chain X1 and X2 Dihedral Angles. *J. Chem. Theory Comput.* **2012**, *8*, 3257−3273.

(24) Jorgensen, W. L.; Chandrasekhar, J.; Madura, J. D.; Impey, R. W.; Klein, M. L. Comparison of Simple Potential Functions for Simulating Liquid Water. *J. Chem. Phys.* **1983**, *79*, 926−935.

(25) Izadi, S.; Anandakrishnan, R.; Onufriev, A. V. Building Water Models: A Different Approach. *J. Phys. Chem. Lett.* **2014**, *5*, 3863−3871.

(26) Dickson, C. J.; Madej, B. D.; Skjevik, A. A.; Betz, R. M.; Teigen, K.; Gould, I. R.; Walker, R. C. Lipid14: The Amber Lipid Force Field. *J. Chem. Theory Comput.* **2014**, *10*, 865−879.

(27) Maier, J. A.; Martinez, C.; Kasavajhala, K.; Wickstrom, L.; Hauser, K. E.; Simmerling, C. ff14SB: Improving the Accuracy of Protein Side Chain and Backbone Parameters from ff99SB. *J. Chem. Theory Comput.* **2015**, *11*, 3696−3713.

(28) Case, D.; Ben-Shalom, I.; Brozell, S.; Cerutti, D.; Cheatham, T., III; Cruzeiro, V.; Darden, T.; Duke, R.; Ghoreishi, D.; Giambasu, G.; Giese, T.; Gilson, M.; Gohlke, H.; Goetz, A.; Greene, D.; Harris, R.; Homeyer, N.; Huang, Y.; Izadi, S.; Kovalenko, A.; Krasny, R.; Kurtzman, T.; Lee, T.; LeGrand, S.; Li, P.; Lin, C.; Liu, J.; Luchko, T.; Luo, R.; Man, V.; Mermelstein, D.; Merz, K.; Miao, Y.; Monard, G.; Nguyen, C.; Nguyen, H.; Onufriev, A.; Pan, F.; Qi, R.; Roe, D.; Roitberg, A.; Sagui, C.; Schott-Verdugo, S.; Shen, J.; Simmerling, C.; Smith, J.; Swails, J.; Walker, R.; Wang, J.; Wei, H.; Wilson, L.; Wolf, R.; Wu, X.; Xiao, L.; Xiong, Y.; York, D.; Kollman, P. *Amber18*; University of California: San Francisco, 2019.

(29) Götz, A. W.; Williamson, M. J.; Xu, D.; Poole, D.; Le Grand, S.; Walker, R. C. Routine Microsecond Molecular Dynamics Simulations with AMBER on GPUs. 1. Generalized Born. *J. Chem. Theor. Comput.* **2012**, *8*, 1542−1555.

(30) Humphrey, W.; Dalke, A.; Schulten, K. VMD: Visual Molecular Dynamics. *J. Mol. Graphics* **1996**, *14*, 33−38.

(31) Romo, T. D.; Leioatts, N.; Grossfield, A. Lightweight Object Oriented Structure Analysis: Tools for Building Tools to Analyze Molecular Dynamics Simulations. *J. Comput. Chem.* **2014**, *35*, 2305−2318.

(32) Williams, T.; Kelley, C. *Gnuplot 5.2: An Interactive Plotting Program*, 2020.

(33) Vostrikov, V. V.; Hall, B. A.; Greathouse, D. V.; Koeppe, R. E.; Sansom, M. S. P. Changes in Transmembrane Helix Alignment by Arginine Residues Revealed by Solid-State NMR Experiments and Coarse-Grained MD Simulations. *J. Am. Chem. Soc.* **2010**, *132*, 5803−5811.

(34) Dorairaj, S.; Allen, T. W. On the Thermodynamic Stability of a Charged Arginine Side Chain in a Transmembrane Helix. *Proc. Natl. Acad. Sci. U.S.A.* **2007**, *104*, 4943−4948.

https://dx.doi.org/10.1021/acs.langmuir.0c02038
Langmuir XXXX, XXX, XXX−XXX

(35) Öjemalm, K.; Higuchi, R. C.; Lara, P.; Lindahl, E.; Suga, H.; von Heijne, G. Energetics of Side-Chain Snorkeling in Transmembrane Helices Probed by Nonproteinogenic Amino Acids. *Proc. Natl. Acad. Sci. U.S.A.* **2016**, No. 201606776.
(36) Patel, S. J.; Van Lehn, R. C. Characterizing the Molecular Mechanisms for Flipping Charged Peptide Flanking Loops across a Lipid Bilayer. *J. Phys. Chem. B* **2018**, *122*, 10337−10348.
(37) Flanagan, J. C.; Baiz, C. R. Site-Specific Peptide Probes Detect Buried Water in a Lipid Membrane. *Biophys. J.* **2019**, *116*, 1692−1700.
(38) Flanagan, J. C.; Cardenas, A. E.; Baiz, C. R. Ultrafast Spectroscopy of Lipid−Water Interfaces: Transmembrane Crowding Drives H-Bond Dynamics. *J. Phys. Chem. Lett.* **2020**, *2020*, 4093−4098.
(39) Vasquez-Montes, V.; Gerhart, J.; Thévenin, D.; Ladokhin, A. S. Divalent Cations and Lipid Composition Modulate Membrane Insertion and Cancer-Targeting Action of pHLIP. *J. Mol. Biol.* **2019**, *431*, 5004−5018.
(40) Schow, E. V.; Freites, J. A.; Cheng, P.; Bernsel, A.; von Heijne, G.; White, S. H.; Tobias, D. J. Arginine in Membranes: The Connection Between Molecular Dynamics Simulations and Translocon-Mediated Insertion Experiments. *J. Membr. Biol.* **2011**, *239*, 35−48.
(41) Karabadzhak, A. G.; Weerakkody, D.; Deacon, J.; Andreev, O. A.; Reshetnyak, Y. K.; Engelman, D. M. Bilayer Thickness and Curvature Influence Binding and Insertion of a pHLIP Peptide. *Biophys. J.* **2018**, *114*, 2107−2115.
(42) Scott, H. L.; Heberle, F. A.; Katsaras, J.; Barrera, F. N. Phosphatidylserine Asymmetry Promotes the Membrane Insertion of a Transmembrane Helix. *Biophys. J.* **2019**, *116*, 1495−1506.
(43) Sodt, A. J.; Pastor, R. W.; Lyman, E. Hexagonal Substructure and Hydrogen Bonding in Liquid-Ordered Phases Containing Palmitoyl Sphingomyelin. *Biophys. J.* **2015**, *109*, 948−955.
(44) Slaybaugh, G.; Weerakkody, D.; Engelman, D. M.; Andreev, O. A.; Reshetnyak, Y. K. Kinetics of pHLIP Peptide Insertion into and Exit from a Membrane. *Proc. Natl. Acad. Sci. U.S.A.* **2020**, *117*, 12095−12100.
(45) Onyango, J. O.; Chung, M. S.; Eng, C.-H.; Klees, L. M.; Langenbacher, R.; Yao, L.; An, M. Noncanonical Amino Acids to Improve the pH Response of pHLIP Insertion at Tumor Acidity. *Angew. Chem., Int. Ed.* **2015**, *54*, 3658−3663.

https://dx.doi.org/10.1021/acs.langmuir.0c02038
Langmuir XXXX, XXX, XXX−XXX